Materials and Manufacturing Processes

ISSN: 1042-6914 (Print) 1532-2475 (Online) Journal homepage: www.tandfonline.com/journals/lmmp20

Prediction of cutting speed interval of diamond-coated tools with residual stress

Mehmet Aydin

To cite this article: Mehmet Aydin (2017) Prediction of cutting speed interval of diamond-coated tools with residual stress, Materials and Manufacturing Processes, 32:2, 145-150, DOI: 10.1080/10426914.2016.1140197

To link to this article: https://doi.org/10.1080/10426914.2016.1140197

MATERIALS AND MANUFACTURING PROCESSES
2017, VOL. 32, NO. 2, 145–150
http://dx.doi.org/10.1080/10426914.2016.1140197

Taylor & Francis
Taylor & Francis Group

Prediction of cutting speed interval of diamond-coated tools with residual stress

Mehmet Aydin

Department of Industrial Product Design, Bilecik Şeyh Edebali University, Bilecik, Turkey

ABSTRACT

This article deals with finite element (FE) analysis incorporating deposition stress effects to determine the optimal cutting speed interval, $\boldsymbol{V}_{\text{interval}}$, and evaluate the effects of cutting speed on the interface behavior of diamond-coated tools in machining of AA356-T6 aluminum alloy. A model for predicting the $\boldsymbol{V}_{\text{interval}}$ limited through the lower, $\boldsymbol{V}_{\text{lower}}$, and upper, $\boldsymbol{V}_{\text{upper}}$, cutting speeds is also presented. The results show that the deposition process causes high residual stress around the round edge on the coating side. When machining load corresponding to the speed interval is applied, the residual stress on the coating side is decreased at the $\boldsymbol{V}_{\text{upper}}$.

ARTICLE HISTORY
Received 14 October 2015
Accepted 3 December 2015

KEYWORDS
Aluminum; coatings; cutting; diamond; numerical; speed; stress; tooling

Introduction

Chemical vapor deposition (CVD) diamond-coated tools are widely employed in machining of high-strength materials. Despite their high strength and low friction properties, the diamond-coated tools are influenced by inadequate coating–substrate adhesion, deposition stress, tool geometry, and machining load. Coating separation is found as the basic deterioration mechanism of CVD diamond-coated tools [1].

Although the establishment of optimal speed limits is important for diamond-coated tools, it is not obvious how the cutting speed influences the performance of diamond-coated tools. Deshayes [2] presented an approach to establish the optimal $\boldsymbol{V}_{\text{interval}}$ for a tool–workpiece pair. In this approach, the optimal $\boldsymbol{V}_{\text{interval}}$ was established by finding its lower and upper values. Ma et al. [3] conducted a set of experiments to establish the spindle speed in high-speed machining of curve-shaped parts made of difficult-to-cut materials. These studies indicate that the cutting speed whose operating interval requires to be carefully chosen is a crucial parameter to investigate machining process. The choice of cutting speed also depends on the cutting forces. Many mechanistic approaches were suggested to model various process geometries [4], surface error profiles [5], and cutting forces [6–8]. In whole situations, these approaches require a serious calibration with expensive experimental tests for a tool–workpiece pair. Researchers have been focused on finite element (FE) modeling due to such restrictions. Wu and Guo [9] developed a three-dimensional FE simulation model to study the effect of tool geometric features and process parameters on cutting forces. In recent years, the Arbitrary Lagrangian Eulerian (ALE) FE method has been implemented to analyze a steady-state cutting process. Arrazola et al. [10] predicted the characteristics of the tool—chip interface with an FE chip formation model based on the ALE technique. Kishawy et al. [11] considered the influences of various edge radii on cutting forces by constructing a two-dimensional FE cutting model including the ALE method.

The FE method is rarely employed to investigate the interfacial deterioration due to the difficultness in modeling the interface behavior of cutting tools. However, the interface stress can affect the performance of diamond-coated tools during machining operations. Therefore, it is necessary to consider the influence of deposition and machining load on the diamond-coated tools. Davim [12] investigated the effect of cutting condition on cutting energy, force, and temperature variations by performing two-dimensional experimental cutting tests with diamond-coated tools. Almeida et al. [13] considered the effect of diamond-coated tool geometry upon the cutting forces in machining hard metal. Qin and Chou [14] proposed a two-dimensional FE model for diamond-coated tools with residual stress. This model was implemented to analyze the effect of cutting-edge geometry. In another study, Qin et al. [15] presented a cohesive interface approach for the determination of coating deterioration in orthogonal cutting with diamond-coated tools.

The literature on FE cutting analysis with CVD diamond-coated tools including residual stress effects caused by the deposition process is very unsatisfactory. In this work, the two-dimensional FE models are established to determine the optimal $\boldsymbol{V}_{\text{interval}}$ in machining of AA356-T6 aluminum alloy using the CVD diamond-coated tool including residual stress effects. The model of determining the optimal $\boldsymbol{V}_{\text{interval}}$ is based on the specific machining forces. First, the influence of the deposition process on the interface behavior around the tool tip is investigated by constructing the FE model of the diamond-coated tool with cohesive interface. Then, the influences of the machining process on the diamond-coated tool with residual stress are studied at the $\boldsymbol{V}_{\text{lower}}$ and $\boldsymbol{V}_{\text{upper}}$, which are determined from the prediction model of the $\boldsymbol{V}_{\text{interval}}$.

CONTACT Mehmet Aydin mehmet.aydin@bilecik.edu.tr Department of Industrial Product Design, Bilecik Şeyh Edebali University, Bilecik 11230, Turkey.

Color versions of one or more of the figures in the article can be found online at www.tandfonline.com/lmmp.

Materials and methods

In this study, the two-dimensional FE simulations of the deposition and cutting processes of the diamond-coated tools with cohesive interface are investigated. The FE method is similar to the approach described in Ref. [15]. The FE model of CVD cutting tool consisting of a substrate and a coating is first prepared for the deposition simulation. Then, this model is converted into an Abaqus input file and cohesive elements are defined to construct the cohesive interface. The CVD diamond-coated tools have 50 and 80 µm edge radii, 0° rake angle, 11° clearance angle, and 15 µm coating thickness on tungsten carbide substrate. The substrate is described as an elastic-plastic material. The coating has the temperature-independent linear-elastic material properties. The cohesive interface utilizes the transaction-separation principle with the normal stiffness of 5×10^6 MPa and the shear stiffness of 5×10^6 MPa. Other cohesive interface properties are also defined as: normal strength $\sigma_{max} = 500$ MPa, shear strength $\tau_{max} = 1 \times 10^5$ MPa, fracture energy $G_f = 100$ J/m^2. Four-node elements (CPE4RT) are employed to discretize the substrate and coating. The cohesive interface is modeled with the four-node cohesive elements (COH2D4). The deposition temperature is initially adjusted to 600°C. This temperature is decreased to 20°C at the end of the deposition process.

After the deposition analysis, a thermo-mechanical FE model of the cutting process is constructed to determine the optimal $\boldsymbol{V}_{interval}$ in machining of AA356-T6 aluminum alloy using the diamond-coated tools with residual stress. The feed rate and depth of cut are 0.3 and 1 mm, respectively. The cutting speed is changed from 1 to 6 m/s by an incremental speed of 0.5 m/s.

Figure 1 illustrates the workpiece and diamond-coated tool with cohesive elements set up in Abaqus/Explicit v6.13. The workpiece is modeled using four-node elements (CPE4RT) to take into account the deformations generated in high-speed cutting. The bottom edge of the workpiece is arrested in y direction. The right and top edges of the tool are also constrained in x and y directions, respectively. During machining, the material moves to the right of the workpiece at cutting speed. An approach is adapted to conduct a steady-state cutting process, which is carried out via adaptive meshing. The inflow, chip flow, and outflow ends are the Eulerian boundaries. All other edges are modeled as the Lagrangian boundaries. The workpiece initial temperature is 20°C. Moreover, the initial state is described for the coating, cohesive elements, and substrate imported from the deposition process. Table 1 lists the thermo-mechanical properties of the substrate, coating, and workpiece materials.

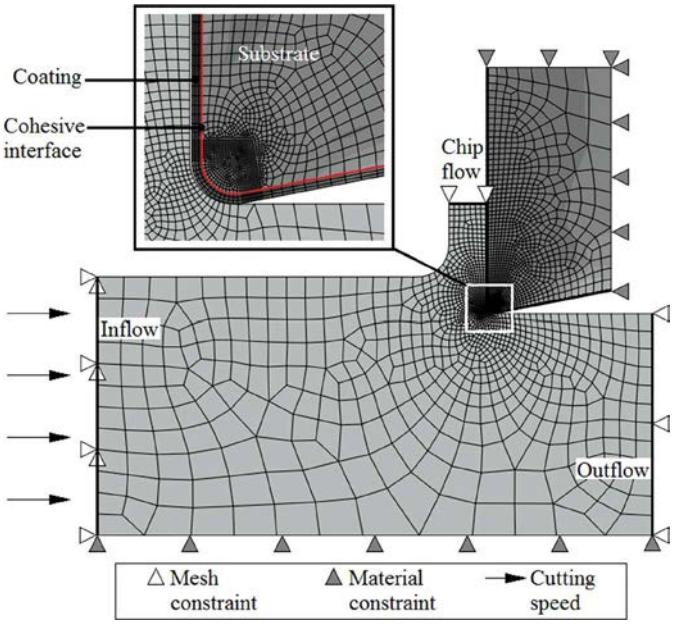

Figure 1. The FE cutting model including cohesive elements.

The behavior of the workpiece material is described using the Johnson–Cook (JC) model [17]:

$$\overline{\sigma} = [477\,\overline{\varepsilon}^{0.144}]\left[1 + 0.0067\ \mathrm{In}\left(\frac{\dot{\overline{\varepsilon}}}{1000}\right)\right]\left[1 - \left(\frac{T-20}{585-20}\right)^{1.62}\right] \quad (1)$$

where the model constants are taken from Ref. [18]. $\overline{\varepsilon}$ is the plastic equivalent strain and the strain rate, $\dot{\overline{\varepsilon}}$, is normalized with a reference strain rate, $\dot{\overline{\varepsilon}}_0$.

Based on Ref. [14], the friction characteristics for the cutting simulations are defined as limited shear stress $\tau_{limit} = 143$ MPa and friction coefficient $\mu = 0.6$.

Finally, a model is considered for determining the optimal $\boldsymbol{V}_{interval}$. The presented model is based on Ref. [2] and uses the specific tangential, K_t, and radial, K_r, force components expressed as follows:

$$\left.\begin{aligned} K_t &= \frac{F_t}{A_c} = \frac{F_t}{a \times f_t} \\ K_r &= \frac{F_r}{A_c} = \frac{F_r}{a \times f_t} \end{aligned}\right\} \quad (2)$$

where F_t and F_r are the tangential and radial force components, respectively. A_c is the chip cross-section area, a is the depth of cut, and f_t is the feed rate.

As expressed in Ref. [2], the K_t values are relatively constant along an interval of cutting speeds. The $\boldsymbol{V}_{lower}$ also corresponds to the minimum K_t value. Considering these explanations, the $\boldsymbol{V}_{lower}$ is described as the speed that corresponds to the minimum value of the K_t. The determination of the $\boldsymbol{V}_{upper}$ is much more problematic. In this study, the K_r is used to establish the $\boldsymbol{V}_{upper}$ value. The $\boldsymbol{V}_{upper}$ is taken as the speed value where the K_r starts to vary after a stable region.

Table 1. The thermo-mechanical properties of the substrate, coating, and workpiece materials [14, 16].

Parameter	AA356-T6 alloy	WC-Co	Diamond
Expansion (m/m°C)	2.14×10^{-5} (at 20°C) 2.32×10^{-5} (at 100°C)	5.5×10^{-6}	2.5×10^{-6}
Density (g/cm^3)	2.67	15.8	3.5
Young's modulus, (N/m^2)	72.4×10^9	620×10^9	1200×10^9
Poisson's ratio	0.33	0.24	0.07
Specific heat (J/kg/°C)	963	2000	509
Conductivity (W/m°C)	151	84.02	900

Results and discussion

Diamond-coated tools having 50 and 80 µm edge radii, 15 µm coating thickness are prepared to perform the deposition stress analysis. Figure 2 illustrates the residual stress contours of the cutting tools. The coordinate system is converted into the cylindrical coordinate system to investigate the residual stress around the round edge. The coordinates 0 and 1 correspond to the start and end points of the round edge, respectively. It can be observed that compressive stress is occurred in the coating, but the substrate has tensile stress around the round edge.

Figure 3 also illustrates the radial, σ_r, and tangential, σ_θ, residual stress distributions on the coating and substrate sides for two different edge radii. It can be seen that the σ_r and σ_θ distributions are mostly compressive on the coating side, but the predicted stress variations are found to be completely tensile on the substrate side. The maximum σ_r value of the coating side is 2.14 GPa for the tool with 50 µm edge radius. This value is very close to the maximum σ_r value, 2.24 GPa, of the coating side predicted for the tool with 80 µm edge radius. The maximum σ_θ values for 50 and 80 µm edge radii are also predicted as 2.22 and 2.48 GPa on the coating side, respectively. These results show that the maximum σr and σ_θ values are in a close range for two different edge radii, but the stress patterns are affected by the edge radii. A similar behavior is also observed at the interface on the substrate side, but the maximum stress values of the substrate side are lesser than the maximum stress values of the coating side. The maximum σ_θ values of the substrate side for 50 and 80 µm edge radii are about 0.5 GPa. The maximum σ_r value corresponding to the substrate side is also found as 0.44 GPa for the tool with 50 µm edge radius and 0.49 GPa for the tool with 80 µm edge radius.

After the deposition analyses, the FE simulations of cutting process are carried out and the prediction model of the speed interval is implemented to establish the $\boldsymbol{V}_{\text{interval}}$ limited through the $\boldsymbol{V}_{\text{lower}}$ and $\boldsymbol{V}_{\text{upper}}$. Figure 4 illustrates the K_t and K_r values as a function of the cutting speed. It is observed that the lowest K_t values for two different radii are obtained at 2 m/s cutting speed and nearly constant between 2 and 2.5 m/s. The K_t values increase at the higher cutting speeds. Thus, the $\boldsymbol{V}_{\text{lower}}$ is 2 m/s.

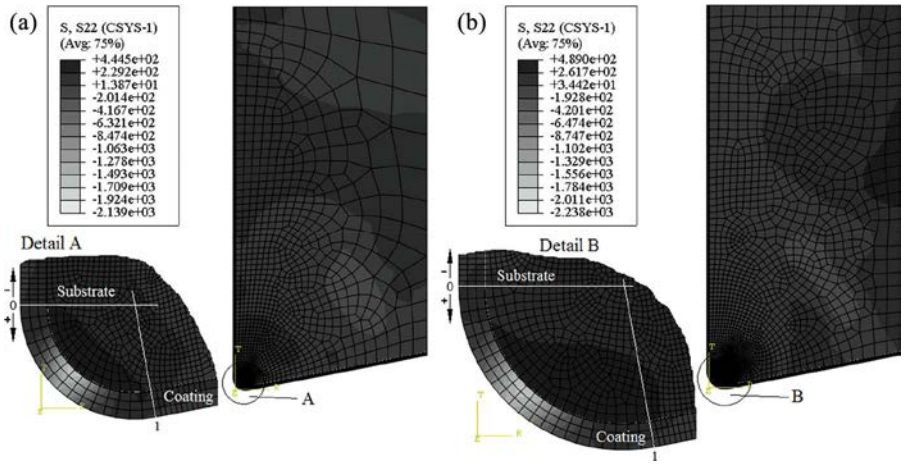

Figure 2. Deposition stress contours in the radial direction (in MPa): a) 50 µm edge radius; b) 80 µm edge radius.

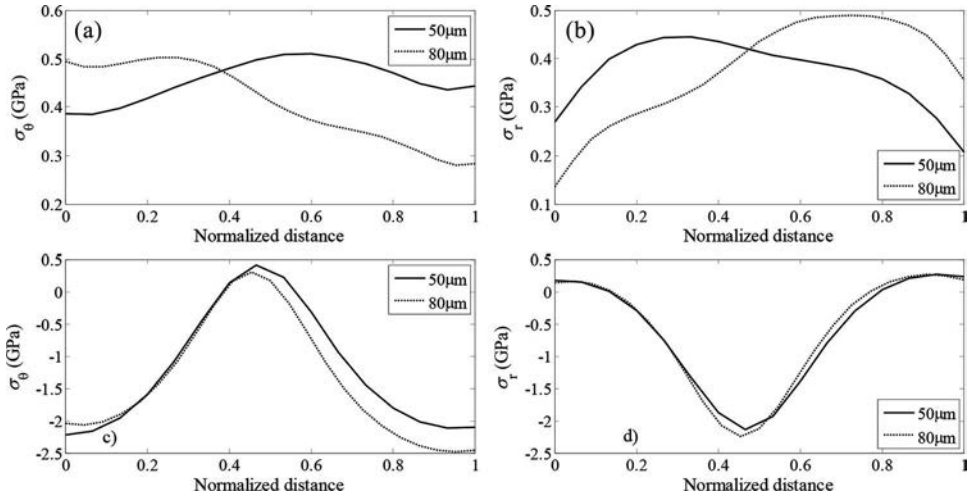

Figure 3. Interface stress profiles around the round edge after the deposition simulation: a) σ_θ; b) σ_r on the substrate side; c) σ_θ; d) σ_r on the coating side.

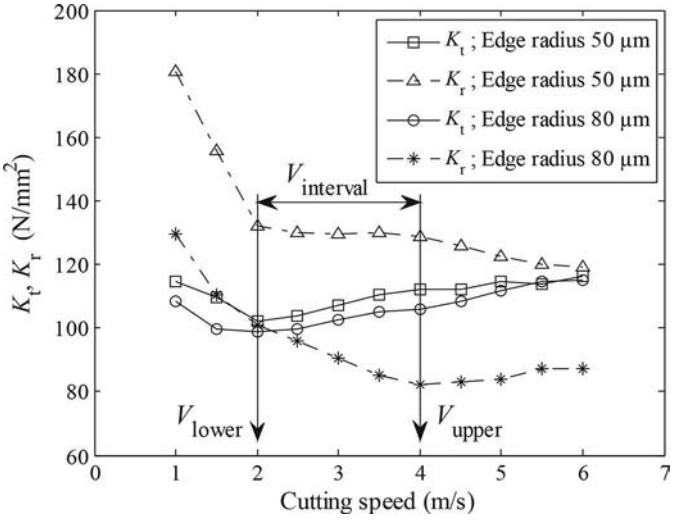

Figure 4. The established cutting speed interval.

The K_r values are investigated to predict the $\boldsymbol{V}_{upper}$. As seen in Fig. 4, the K_r values found for the tool with 50 µm edge radius are nearly constant between 2 and 4 m/s and decrease at cutting speeds above 4 m/s. The K_r values calculated for the tool with 80 µm edge radius also begin to remain stable at 4 m/s. Thus, this intersection that corresponds to 4 m/s is determined as the $\boldsymbol{V}_{upper}$. Further, it can be inferred from the K_t and K_r values that the tool with 50 µm edge radius exhibits a more robust behavior.

As explained earlier, the diamond-coated tool with 50 µm edge radius has more specific machining forces. Therefore, stress analysis with the deposition and machining load is performed on this tool. Figure 5 illustrates the von Mises stress contours obtained at the $\boldsymbol{V}_{upper}$. It can be observed that the highest stress value on the chip is significantly lower than the highest tool stress. The stress values in the primary deformation zone are approximately between 300 and 460 MPa. The tool has a localized stress larger than 5 GPa. It can be deduced that the deposition stress is still effective and varied by the cutting load.

Figure 6 illustrates the interfacial stress distributions along the round edge for the $\boldsymbol{V}_{lower}$ and $\boldsymbol{V}_{upper}$ established earlier. It is seen that cutting speed affects the σ_r and σ_θ, which are critical in coating separation. The σ_r on the substrate side is relieved toward the end of the round edge close to the flank face at the $\boldsymbol{V}_{upper}$. This case can be attributed to the thermal influence arising with increasing cutting speed. The σ_θ also indicates a phenomenon similar to the σ_r. It is clear that the $\boldsymbol{V}_{upper}$ tends to decrease the σ_r and σ_θ on the substrate side. As seen from Fig. 6b, the stress components on the coating side are varied toward tensile after the simulation at the $\boldsymbol{V}_{upper}$.

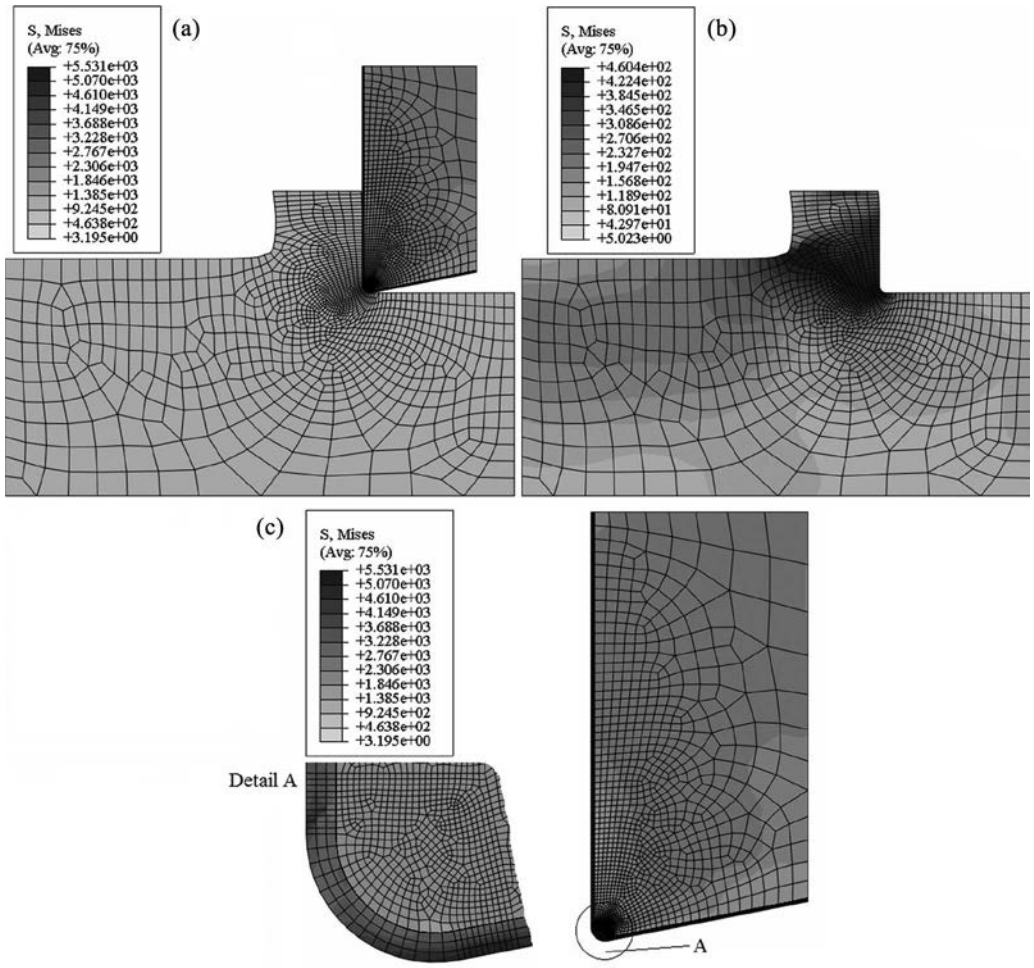

Figure 5. Von Mises stress contours obtained at the $\boldsymbol{V}_{upper}$: a) tool, workpiece, and chip; b) workpiece and chip; c) tool.

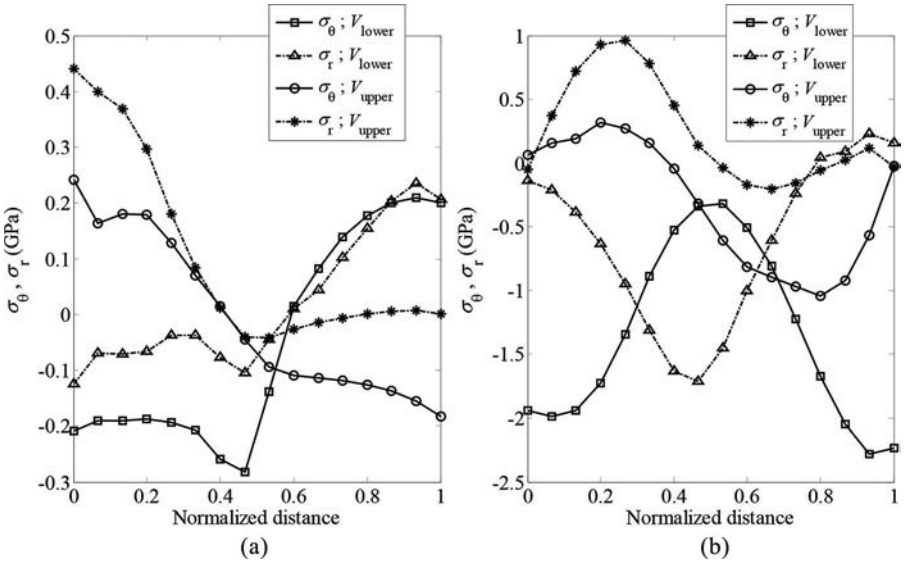

Figure 6. Interface stress profiles along the round edge after the cutting simulation: a) substrate side; b) coating side.

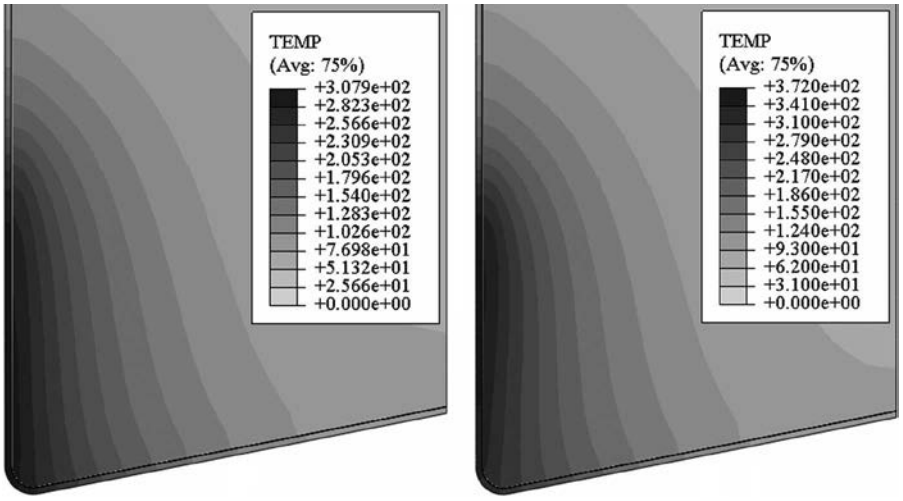

Figure 7. Cutting tool temperatures: a) V_{lower}; b) V_{upper}.

Furthermore, the σ_r and σ_θ are obtained to be the low compressive stress at the end of the round edge close to the flank face since the stress relief exceeds the mechanical contact stress caused by the chip. It can be deduced that the V_{upper} also has a tendency to relieve the σ_r and σ_θ on the coating side.

As seen in Fig. 6b, the σ_θ distribution on the coating side is obtained as completely compressive after the cutting simulation at the V_{lower}. The σ_r variation is mostly compressive without a significant variation. Accordingly, the high compressive stress values on the coating side are still effective at the V_{lower}.

Figure 7 illustrates the predicted tool temperatures at the V_{lower} and V_{upper}. The tool temperatures are typically low and the cutting speed governs temperature rise. When cutting speed is changed from the V_{lower} to the V_{upper}, the maximum tool temperature is found as 372°C for the V_{upper} and 307°C for the V_{lower}. It can be observed from Fig. 7a that the maximum temperature region at the V_{lower} is extended from the round edge to the rake face. This is probably due to the bulk material compressed beneath the tool and the chip flowing toward the rake face. As illustrated in Fig. 7b, the region of the high temperature concentrates at the V_{upper} occurs at some distance from the tool tip on the rake face due to increased temperature of the chip.

Conclusions

In this study, the two-dimensional FE models are constructed to evaluate the optimal V_{lower} and V_{upper} in machining of AA356-T6 aluminum alloy using the CVD diamond-coated tool, including residual stress effects. The model of predicting optimal V_{lower} and V_{upper} is based on the specific machining forces. The deposition stress around the round edge is first analyzed by modeling the diamond-coated tools with different edge radii. The cutting simulations are then conducted to determine the optimal

V_{lower} and V_{upper} for the tool−workpiece pair. The following findings can be concluded from this investigation:

1. At the end of the deposition analysis, the σ_r and σ_θ are obtained as tensile on the substrate side, but these stress components are generally compressive on the coating side. The maximum σr and σ_θ on the substrate side are about 0.5 GPa for two different edge radii. The maximum residual stress components of the coating side are as high as about 2 GPa for two different edge radii. It can be concluded that when the edge radius is varied from 50 to 80 μm, it has a slight influence on the maximum σ_r and σ_θ.
2. From the prediction model of the speed interval, the optimal V_{lower} and V_{upper} are found to be 2 and 4 m/s, respectively. The diamond-coated tool with 50 μm edge radius has a more robust effect on K_t and K_r.
3. According to the von Mises stress results, the highest tool stress is considerably greater than the highest stress value on the chip.
4. When the machining load is applied on the tool with 50 μm edge radius at the V_{lower}, the high compressive stress is still effective on the coating side. After the simulation at the V_{upper}, the σ_r and σ_θ on the coating side are varied toward tensile and relieved due to the thermal influence caused by the increase in cutting speed. Consequently, the V_{upper} has a tendency to decrease the residual stress on the coating side.
5. When cutting speed is increased from the V_{lower} to the V_{upper}, the maximum temperature rise in the cutting tool is approximately 20% and the maximum temperature region is achieved at some distance from the cutting tool tip on the rake face. Accordingly, the tool temperatures are sensitive to the established V_{lower} and V_{upper}.

References

[1] Chou, Y.K.; Liu, J. CVD diamond tool performance in composite machining. *Surface and Coatings Technology* **2005**, *200*, 1872–1878.

[2] Deshayes, L. Analysis of an equivalent tool face for the cutting speed range prediction of complex grooved tools. *Journal of Materials Processing Technology* **2007**, *190*, 251–262.

[3] Ma, J.; Jia, Z.; Wang, F.; Ning, F. Spindle speed selection for high-speed milling of titanium alloy curved surface. *Materials and Manufacturing Processes* **2014**, *29*, 364–369.

[4] Desai, K.A.; Rao, P.V.M. On cutter deflection surface errors in peripheral milling. *Journal of Materials Processing Technology* **2012**, *212*, 2443–2454.

[5] Aydın, M.; Uçar, M.; Cengiz, A.; Kurt, M. Identification of static surface form errors from cutting force distribution in flat-end milling processes. *Journal of the Brazilian Society of Mechanical Sciences and Engineering* **2015**, *37*, 1001–1013.

[6] Wang, B.S.; Zuo, J.M.; Wang, M.L.; Hou, J.M. Prediction of milling force based on numerical simulation of oblique cutting. *Materials and Manufacturing Processes* **2012**, *27*, 1011–1016.

[7] Aydın, M.; Uçar, M.; Cengiz, A.; Kurt, M.; Barkın, B. A methodology for cutting force prediction in side milling. *Materials and Manufacturing Processes* **2014**, *29*, 1429–1435.

[8] Srinivasa, Y.V.; Shunmugam, M.S. Mechanistic model for prediction of cutting forces in micro end-milling and experimental comparison. *International Journal of Machine Tools and Manufacture* **2013**, *67*, 18–27.

[9] Wu, H.; Guo, L. Machinability of titanium alloy TC21 under orthogonal turning process. *Materials and Manufacturing Processes* **2014**, *29*, 1441–1445.

[10] Arrazola, P.J.; Ugarte, D.; Dominguez, X. A new approach for the friction identification during machining through the use of finite element modeling. *International Journal of Machine Tools and Manufacture* **2007**, *48*, 173–183.

[11] Kishawy, H.A.; Deiab, I.M.; Haglund, A.J. Arbitrary Lagrangian Eulerian analysis on cutting with a honed tool. *Proceedings of the Institution of Mechanical Engineers, Part B: Journal of Engineering Manufacture* **2008**, *222*, 155–162.

[12] Davim, J.P. *Traditional Machining Processes. Research Advances*, Springer-Verlag: New York, USA, 2015; p. 33–48.

[13] Almeida, F.A.; Oliveira, F.J.; Sousa, M.; Fernandes, A.J.S.; Sacramento, J.; Silva, R.F. Machining hardmetal with CVD diamond direct coated ceramic tools: effect of tool edge geometry. *Diamond and Related Materials* **2005**, *14*, 651–656.

[14] Qin, F.; Chou, Y.K. 2D Cutting simulations with a diamond-coated tool including deposition residual stresses. *Transactions of the North American Manufacturing Research Institution of SME* **2010**, *38*, 1–8.

[15] Qin, F.; Shen, N.; Chou, K. Implementing a cohesive zone interface in a diamond-coated tool for 2D cutting simulations. In *Proceedings of the ASME 2012 International Mechanical Engineering Congress & Exposition*, Houston, USA, November 9–15, 2012.

[16] Dias, A.M.S.; Modenesi, P.J.; Godoy, G.C. Computer simulation of stress distribution during vickers hardness of WC-6Co. *Materials Research* **2006**, *9*, 73–76.

[17] Johnson, G.R.; Cook, W.H. A constitutive model and data for metals subjected to large strains, high strain rates and high temperatures. In *Proceedings of the 7th International Symposium on Ballistics*, The Hague, The Netherlands, April 19–21, 1983.

[18] Sartkulvanich, P.; Sahlan, H.; Altan, T. A finite element analysis of burr formation in face milling of a cast aluminum alloy. *Machining Science and Technology* **2007**, *11*, 157–181.